# A Portable Brain-Computer Interface Using Micro-Display for Future Mobile Communication System

Xi Zhao[1,2], Guiying Xu[1,2], and Honglin Hu[1,2](✉)

[1] University of Chinese Academy of Sciences, Beijing 100049, China
[2] Shanghai Advanced Research Institute, Chinese Academy of Sciences, Beijing, China
huhl@sari.ac.cn

**Abstract.** 5G is gradually realizing low latency and high reliable transmission between devices. In the next-generation mobile communication system, in addition to the further evolution for conventional communication technology, a new way of human-machine communication (HMC) represented by brain-computer interfaces (BCIs) will appear to achieve more efficient human-machine communication. BCIs based on steady-state visual evoked potential (SSVEP) are becoming one of the most popular research direction because of its high accuracy and less dependency on data training. However, the implementation of SSVEP-BCIs depends on external visual stimuli which usually use computer monitor to display the external stimuli. Therefore, this kind of BCIs usually has poor portability and wearability. This disadvantage is hindering the combination of BCIs based on SSVEP and specific control scenarios such as aircraft control, which require high wearability of control devices. The current portable schemes usually make use of the binocular effect and AR glasses to improve portability but no BCI system has been designed by making full use of the conclusion that stimulating single eye can also stimulate the brain to produce strong responses. In order to improve the portability of the BCIs based on SSVEP, a monocular-based scheme is proposed in this study. A brain-controlled aircraft system based on SSVEP is designed to verify the feasibility of this wearable scheme.

**Keywords:** BCI · SSVEP · AR

## 1 Introduction

According to the current progress of 5G research and application, 5G has been applied to the following three usage scenarios: enhanced mobile broadband (eMBB), massive machine-type communications (mMTC), and ultrareliable low-latency communications (URLLC) [1]. In particular, eMBB successfully realizes the efficient transmission of data between users, mMTC focuses on the highly reliable connection between a large number of machines in the Internet of things

© ICST Institute for Computer Sciences, Social Informatics and Telecommunications Engineering 2022
Published by Springer Nature Switzerland AG 2022. All Rights Reserved
C. T. Calafate et al. (Eds.): MONAMI 2021, LNICST 418, pp. 3–16, 2022.
https://doi.org/10.1007/978-3-030-94763-7_1

(IoT), and URLLC is applied to the real-time scenarios with low-latency and high-reliability represented by vehicle networking. These scenarios are gradually realizing the information communication with high efficient between devices.

Although the mentioned 5G technology has been gradually applied to various industries to improve the quality of our life, the conventional keyboard and mouse communication method is still used in the human-machine communication (HMC) between users and external devices. It can be predicted that exploring more efficient HMC methods will be one of the most important research direction of the next-generation mobile communication. With the exploration of the brain mechanism, brain-computer interface (BCI) is becoming a high-profile research direction of the HMC schemes. At present, BCI technology is considered to have a great prospect in the field of IoT to realize smart healthcare [2], and to replace the conventional HMC tools such as keyboard and mouse to control external devices.

BCIs can help users to interact with the machine directly via using the neural activities [3]. The ultimate goal of BCIs is to achieve more efficient human-machine interface and liberate human hands. At present, BCIs have realized several application scenarios, such as medical auxiliary rehabilitation [4], disease surveillance, auxiliary control external equipment [5], etc. With the further exploring of the paradigm of BCIs in recent decades, the BCIs based on steady-state visual evoked potential (SSVEP) are becoming one of the most famous BCI paradigms because of its high signal-to-noise ratio (SNR) and observable features [6].

The primary visual cortex of brain will produce specific responses which is highly correlated with the stimulus frequency, when the user is gazing at a visual stimulus flashing with a specific frequency. The neural responses can be recorded by the electroencephalogram (EEG, a common non-invasive brain responses acquisition scheme), so that the data processing unit can further process the collected neural data. Then, the collected neural data can be detected after corresponding processing. Finally, the detection results will be mapped to the control commands to control the external device. Compared with other types of BCIs like P300 [7,8], motor imagery [9,10] and slow cortical potential [11], SSVEP-BCIs [12] can stimulate the brain to produce a more stable response, so this kind of BCIs can usually achieve the highest information transfer rate (ITR). At present, the BCIs based on SSVEP have realized several application scenarios such as keyboard typing [13], aircraft control [5], robotic arm control [14], etc.

David and Berndt proposed in [15] that interactive devices which can inspire users to buy and use in the next-generation mobile communication era must be portable. However, as described above, the SSVEP-BCIs usually require additional monitors to display the external stimuli. This disadvantage leads to poor portability and wearability of SSVEP-BCIs. Poor portability is hindering the further application of SSVEP-BCIs in control scenarios that require high device portability, such as aircraft control. Some recent studies have used augmented reality (AR) technology to improve the portability of SSVEP-BCIs. In the paper [16], the authors have successfully verified that the SSVEP stimulation presented

by AR smart glasses can be used in the field of BCIs. Furthermore, a robot control system based on SSVEP-BCIs is realized by using AR glasses [17]. The scheme of using AR glasses to display external stimulation in the industrial manufacturing workshop helps the SSVEP-BCIs to control the machine tools [18]. The aboved studies have shown that the combination of AR technology and BCIs can effectively improve the portability and wearability of SSVEP-BCIs.

However, the above-mentioned SSVEP-BCIs are based on binocular vision, there are no monocular vision-based portable BCIs. [19] has been proved that there is no significant difference between monocular and binocular vision under SSVEP stimulation. In order to further improve the portability and wearability of SSVEP-BCI equipments on the basis of the above schemes, a monocular micro-display based on AR technology is used to display the external stimuli in this study. In application such as UAV control, we usually hope that any user can directly control the UAV after wearing the devices. Therefore, data training will reduce the user experience. UAV usually needs to fly in the open air, which means that the light can interfere with visuli stimuli. Thus, the decoding algorithm is required to have nice environmental robustness. In addition, due to the need to process the EEG signal in real time, the algorithm with high complexity is not suitable for such online system. An aircraft control system using SSVEP signal detection method based on canonical correlation analysis (CCA) [20] is designed to verify the feasibility of the proposed stimulation display scheme.

This paper proceeds as the following sections. The Sect. 2 will introduce the hardware platform of the aircraft control system and the features of SSVEP signals. The Sect. 3 will describe the overall architecture of the control system and the neural signal detection algorithm. In the Sect. 4, we will show the performance of the brain-control system under the monocular micro-display scheme. The summary and future vision are presented in the Sect. 5.

## 2 Hardware Platform

### 2.1 Aircraft

The DJI MAVIC AIR quadcopter (Fig. 1(a)) is selected as the terminal to present the control instructions of the brain control system. This kind of quadcopter has the advantages of small size, supporting WiFi connection and allowing the secondary development of Android and Windows. Furthermore, the aircraft supports automatic obstacle avoidance, real-time image transmission, low-power automatic return and other safety functions. These safety functions effectively provided a guarantee for the hidden of dangers caused by the unstable factors introduced by the brain control of the BCIs. The Windows SDK provided by DJI is used to realize the mapping of brain control commands to aircraft control operations.

### 2.2 AR Monocular Micro-Display

A monocular micro-display (Mad gaze-$\chi$5 smart glasses) based on AR technology is used to display the external SSVEP stimuli (Fig. 1(b)). The micro-display

(a) (b) (c)

**Fig. 1.** The equipments that the user needs to wear when controlling the aircraft.

weighs 70 g and has a resolution of 800 × 480 with a refresh rate 60 Hz. The device is usually worn in the right eye (Fig. 2). When the user uses the micro-display to control the aircraft, the SSVEP stimuli will be displayed in the form of video in the above-mentioned micro-display. Table 1 compares the weight, size and wearability of three kinds of SSVEP stimulation display schemes. From the comparison, the proposed scheme has the best portability and wearability.

**Table 1.** Three stimulation display schemes of SSVEP-BCIs. ✗ indicates that the scheme is not wearable. ✔ indicates that the scheme is wearable.

| Display type | Weight | Size | Wearability |
|---|---|---|---|
| LCD display | 2700 g | 23.8 in | ✗ |
| AR smart glasses | 129 g | 0.8 in × 2 | ✔ |
| Monocular micro-display | 70 g | 0.5 in | ✔ |

### 2.3 Neural Data Acquisition Device

Neural data are collected using a 64-channel Quick-Cap provided by Neuroscan Fig. 1(c). 11 electrodes are selected to record the neural data (one reference electrode, one GND electrode), and these electrodes are placed in the standard electrode position (PZ, POZ, PO3, PO4, PO5, PO6, OZ, O1, O2, GND, REF), as shown in Fig. 3. The sample rate of the sensor is set 1000 Hz. The neural data of all channels need to be processed by a bandpass filter 3 Hz 40 Hz before detection to reduce the linear noise.

### 2.4 SSVEP Stimulation Design

The joint frequency-phase modulation (JFPM) method [21] is used to present visual flicker stimuli on the micro-display (Fig. 1(b)). The stimuli can be generated by

$$s = \frac{1}{2} + \frac{1}{2} \times \sin\left(2\pi f(\frac{t}{\text{Refresh Rate}}) + \phi\right), \tag{1}$$

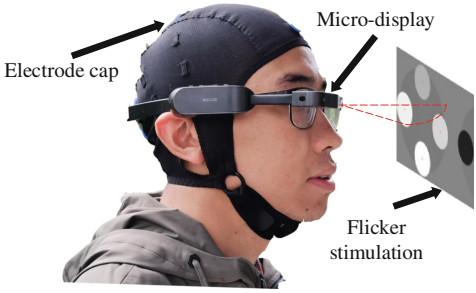


**Fig. 2.** The equipments that the user needs to wear when controlling the aircraft.

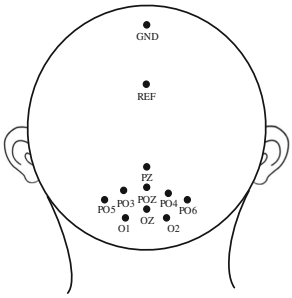


**Fig. 3.** Electrode map of neural data acquisition equipment.

where $f$ and $\phi$ are the frequency and phase of the scintillation stimulus, respectively. $t$ indicates the frame index in the stimulus sequence. Five rounded stimuli are used to encode five flight commands of the aircraft. The dynamic range of the stimulation signal is from 0 to 1, where 0 represents complete darkness and 1 represents the highest luminance. The radius of each flicker stimulus is 280 pixels. Figure 4 depicts the corresponding frequencies of the five flicker stimuli, the aircraft control instructions corresponding to each flicker target, and the spatial position on the micro-display. The stimulus program was established under MATLAB (MathWorks, Inc.) using the physics Toolbox Version 3 [22].

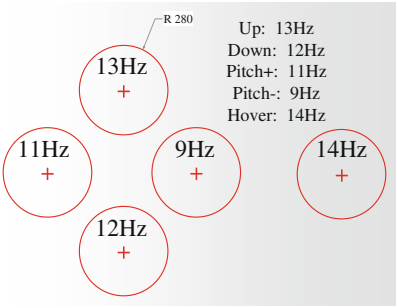


**Fig. 4.** The control interface on the micro-display. The red cross in each flashing target is the area that the user needs to gaze when using the micro-display to control the aircraft. (Color figure online)

### 2.5 The Features of SSVEP

When the subjects are gazing at the flicker stimulus at a specific frequency, the external cortex corresponding to the primary visual area of the brain will produce fundamental responses and harmonic waves as the same frequency as the visual stimulus. The features can be more obvious via calculating the amplitude response of the discrete Fourier transform (DFT) of the neural data collected from a certain channel. The amplitude response of the OZ channel is shown in Fig. 5 when the data length is 5 s and the frequency of the stimulus 7 Hz. The fundamental wave with the same frequency as the stimulus is marked by the red circle, and the green circle marks the high-order harmonics with the same frequency doubling as the stimulus.

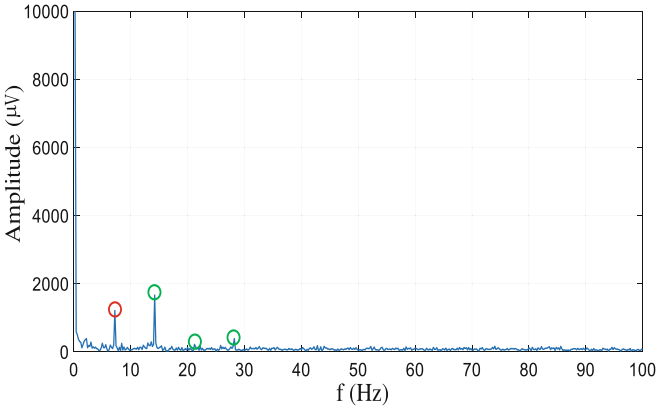


**Fig. 5.** Amplitude response of OZ channel in cerebral cortex when the stimulus frequency 7 Hz.

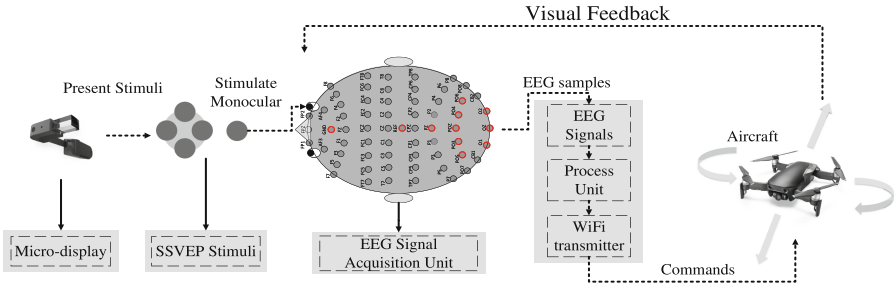


**Fig. 6.** System architecture of the brain-controlled aircraft based on SSVEP-BCIs.

## 3 Software Implementation

### 3.1 System Architecture

The structure of the aircraft control system is shown in Fig. 6. The user wears the micro-display and chooses to gaze at the flicker target in the micro-display according to the specific operation user wants the aircraft to perform. The signals generated induced by the visual stimuli will be recorded by the neural signal recording devices, and these recorded signals will be transmitted to the computer for processing and detection. Finally, the detection results will be transmitted to the aircraft via WiFi, and the aircraft will perform the corresponding commands.

### 3.2 Detection Algorithm

The aircraft needs to work in a open outdoor environment. Meanwhile, asynchronous control is usually required for this kind of control system. Thus, we use the CCA detection algorithm based on sine and cosine reference signal, which does not need data training and has good environment robustness [20]. In this method, the collected neural data is represented by $\boldsymbol{s} \in \boldsymbol{R}^{N_c \times N_t}$, where $N_c$ is the number of electrode channels and $N_t$ is the length of neural data in each channel. The reference signal can be set as

$$\boldsymbol{r}(t) = \begin{pmatrix} \boldsymbol{r}_1(t) \\ \boldsymbol{r}_2(t) \\ \boldsymbol{r}_3(t) \\ \boldsymbol{r}_4(t) \\ \cdots \\ \cdots \\ \boldsymbol{r}_{2N_h-1}(t) \\ \boldsymbol{r}_{2N_h}(t) \end{pmatrix} = \begin{pmatrix} \sin(2\pi ft) \\ \cos(2\pi ft) \\ \sin(2 \times 2\pi ft) \\ \cos(2 \times 2\pi ft) \\ \cdots \\ \cdots \\ \sin(N_h \times 2\pi ft) \\ \cos(N_h \times 2\pi ft) \end{pmatrix} \quad (2)$$
$$, t = 1/L, 2/L, ..., T/L,$$

where $f$ is the frequency of stimuli, $T$ is the number of sampling points, $L$ is the sampling rate (according to Sect. 2.3, $L = 1000$) and $N_h$ is the number

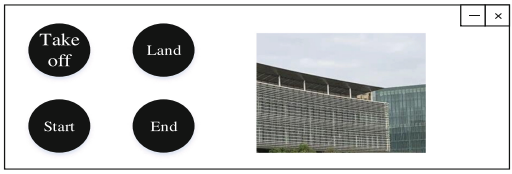


**Fig. 7.** Control interface of aircraft on PC.

of harmonic waves ($N_h = 5$ in this study). The purpose of the neural signal detection algorithm based on CCA is to find two sets of coefficients $\boldsymbol{w}_s \in \boldsymbol{R}^{N_c}$ and $\boldsymbol{w}_r \in \boldsymbol{R}^{2N_h}$ to satisfy the following:

$$\max \rho = \frac{E(\boldsymbol{w}_s^T \boldsymbol{s} \boldsymbol{w}_r^T \boldsymbol{r})}{\sqrt{E(\boldsymbol{w}_s^T \boldsymbol{s}) E(\boldsymbol{w}_r^T \boldsymbol{r})}}, \tag{3}$$

where $\boldsymbol{s}$ is the collected neural signal and $\boldsymbol{r}$ is the reference signal which can be generated from Eq. (2). The final detection results can be calculated as

$$f_s = \max_f \rho(f), \quad f = f_1, f_2, ..., f_5, \tag{4}$$

where $f_1, f_2, ..., f_5$ are the frequencies of the visual stimuli. In the actual aircraft use scenario, it is not necessary to output commands to the aircraft all time. The aircraft needs to keep hovering when the user state is idle. Thus, the control instructions will be mapped to the aircraft only if

$$\rho > \gamma. \tag{5}$$

If Eq. (5) is not satisfied, the aircraft only maintain hovering.

### 3.3 Operation Instruction

In this study, a desktop application based on C# programming environment is designed to realize the mapping between the detection results of neural signals and the control instructions of aircraft. The interface of the desktop platform is shown in Fig. 7. When users use the BCI system to control the aircraft, they need to go through the following operations:

- The user should wear the micro-display and EEG electrode cap and check if the devices are securely worn.
- The conductive medium needs to be injected into the electrode channels of the electrode cap to establish a stable connection between the electrode cap and scalp.
- The aircraft control platform at PC should be opened, and the deployment of aircraft needs to be completed via click the take-off button.
- The aircraft will enters the brain control mode if the start button is clicked. In this mode, the user can choose to gaze at the corresponding visual stimuli according to their own needs, and the aircraft will execute the corresponding control instructions.

### 3.4 Emergency Response

In practical application scenarios, aircraft needs to adapt to different work environments. Therefore, the brain-controlled aircraft is set up as follows:

- When the distance between the aircraft and the user exceeds the maximum control distance of the WiFi, the aircraft will automatically return.
- When the power of the aircraft is too low, the aircraft will automatically return to ensure safety.
- All emergency obstacle avoidance functions are activated so that users can safely control aircraft in complex environments.
- When the user exits the brain control mode, the aircraft will automatically return.

## 4 Results and Analysis

### 4.1 The Description of Online Experiment

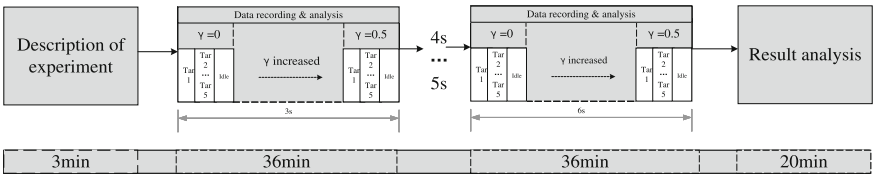


**Fig. 8.** The flow of online experiment.

An online BCI experiment is designed to verify the feasibility of the micro-display scheme. In order to be consistent with the user's normal use of aircraft, the experiments were carried out outside on a sunny day with normal ligh illumination (400 lux to 1000 lux). Four subjects participated in the online experiment. All subjects were asked to read and sign an informed consent form before the formal experiment, and the corresponding rewards were given to all subjects after experiments. All EEG experiments were approved by the Ethics Committee of ShanghaiTech university.

Before the formal experiment, all subjects were informed of the process of the experiment. The online experiment verifies the feasibility of the micro-display-assisted display scheme when the time window is set as 3 s, 4 s, 5 s, 6 s. The detailed experiment flow is shown in Fig. 8. Under each time window and each threshold value $\gamma$, the subjects gazed at each flicker target for 1 min and recorded the flight posture of the aircraft. The one flicker target correspond to one flight command of the aircraft. Thus, other flight attitudes which do not correspond to the flicker target are recorded as the wrong flight commands. When the gaze tasks of all targets are completed under the same time window and the same threshold

value $\gamma$, the subject remained idle for one minute, at which time any flight attitudes of the aircraft except hovering are recorded as the wrong command. The subject would keep gazing at all targets repeatedly and switching to remain idle until the data collection of all the time window and threshold value $\gamma$ were completed.

### 4.2 The Paradigms of Idle State Detection

The accuracy of the detection algorithm for all subjects are shown in Table 2 to Table 5 under different time windows and different idle thresholds $\gamma$. The detection accuracy can be calculated as

$$acc = \frac{C_r}{C_r + C_w} \cdot 100 \quad (\%) \tag{6}$$

where $C_r$ and $C_w$ represent the number of correct commands and wrong commands respectively. The detection algorithm could not effectively identify the idle state of all subjects when $\gamma = 0, 0.1, 0.2$. The idle state of all subjects could be identified when the threshold value $\gamma = 0.3$. But the idle state of S2 and S4 could not be effectively recognized when $\gamma = 0.4$. All subjects were unable to output normal operation instructions when the threshold value $\gamma \geq 0.5$. According to the description of the above results, it can be concluded that the correlation between the SSVEP signals generated by the brain excited the monocular micro-display and the reference signals in the CCA detection algorithm based on sine and cosine wave is between 0.2 and 0.5. The threshold value $\gamma$ and the time window of collected neural signals need to be adjusted according to the EEG signal quality of different users, so as to ensure a better user experience.

### 4.3 The Detection Performance

As can be seen from Fig. 9, the highest average signal recognition accuracy is achieved when the time window is 6 s and the threshold value $\gamma = 0.3$ (83.15%).

**Table 2.** The accuracy of subject 1 detected by the algorithm under different time window and threshold values $\gamma$. ✓ indicates that the idle state detection of the subject can be realized under this time window and threshold value $\gamma$.

| S1 | 3 s | 4 s | 5 s | 6 s |
|---|---|---|---|---|
| $\gamma = 0$ | 57.8% | 55.9% | 71.1% | 61.4% |
| $\gamma = 0.1$ | 50.7% | 54.7% | 57.4% | 62.7% |
| $\gamma = 0.2$ | 55.9% | 52% | 88.5% | 58.5% |
| $\gamma = 0.3$ | 65.6% ✓ | 62.9% ✓ | 76.6% ✓ | 100% ✓ |
| $\gamma = 0.4$ | 84.5% ✓ | 82.7% ✓ | 97.8% ✓ | 92.8% ✓ |
| $\gamma = 0.5$ | 0 | 0 | 0 | 0 |

**Table 3.** The accuracy of subject 2 detected by the algorithm under different time window and threshold values $\gamma$. ✓ indicates that the idle state detection of the subject can be realized under this time window and threshold value $\gamma$.

| S2 | 3 s | 4 s | 5 s | 6 s |
|---|---|---|---|---|
| $\gamma = 0$ | 36.7% | 52.4% | 57.5% | 51.1% |
| $\gamma = 0.1$ | 54.7% | 41.0% | 41.0% | 61.0% |
| $\gamma = 0.2$ | 41.3% | 55.8% | 53.7% | 53.1% |
| $\gamma = 0.3$ | 38.3% | 62.2% ✓ | 62.2% ✓ | 73.4% ✓ |
| $\gamma = 0.4$ | 30.8% | 0 | 0 | 0 |
| $\gamma = 0.5$ | 0 | 0 | 0 | 0 |

**Table 4.** The accuracy of subject 3 detected by the algorithm under different time window and threshold values $\gamma$. ✓ indicates that the idle state detection of the subject can be realized under this time window and threshold value $\gamma$.

| S3 | 3 s | 4 s | 5 s | 6 s |
|---|---|---|---|---|
| $\gamma = 0$ | 56.1% | 71.4% | 71.1% | 78.6% |
| $\gamma = 0.1$ | 48.8% | 68.4% | 68.9% | 61.4% |
| $\gamma = 0.2$ | 61.9% | 61.9% | 55.3% | 74% |
| $\gamma = 0.3$ | 62.5% ✓ | 67.4% ✓ | 90.2% ✓ | 87.2% ✓ |
| $\gamma = 0.4$ | 71.1% ✓ | 78.9% ✓ | 97% ✓ | 94.1% ✓ |
| $\gamma = 0.5$ | 0 | 0 | 0 | 0 |

S1 achieved the best accuracy (100%) when the time window was 6 s and $\gamma = 0.3$, while the recognition accuracy of S3 is 73.4%. The above experimental results show that the subjects can control the aircraft stably in outdoors with complex light interference via using the proposed scheme. This conclusion fully proves that the scheme proposed in this study is feasible.

## 5 Discussion and Conclusion

In this study, the CCA-based detection algorithm with correlation coefficient threshold can obtain high accuracy (Fig. 9) under aircraft control scenario. Due to the optimization of this algorithm, some poor quality neural signals only correspond to the hovering operation of the aircraft, which corresponds to a more reliable control of the aircraft. According to the oral evaluation of the four subjects, they were more willing to use the micro-display to display the extra stimulation rather than computer display.

**Table 5.** The accuracy of subject 4 detected by the algorithm under different time window and threshold values $\gamma$. ✓ indicates that the idle state detection of the subject can be realized under this time window and threshold value $\gamma$.

| S4 | 3 s | 4 s | 5 s | 6 s |
|---|---|---|---|---|
| $\gamma = 0$ | 71.4% | 59.2% | 68.3% | 71.8% |
| $\gamma = 0.1$ | 69.1% | 51.1% | 72.1% | 70.3% |
| $\gamma = 0.2$ | 61.1% | 61.1% | 65.9% | 70.0% |
| $\gamma = 0.3$ | 65.9% ✓ | 63.1% ✓ | 78.3% ✓ | 94.4% ✓ |
| $\gamma = 0.4$ | 81.8% ✓ | 0% | 0% | 0% |
| $\gamma = 0.5$ | 0 | 0 | 0 | 0 |

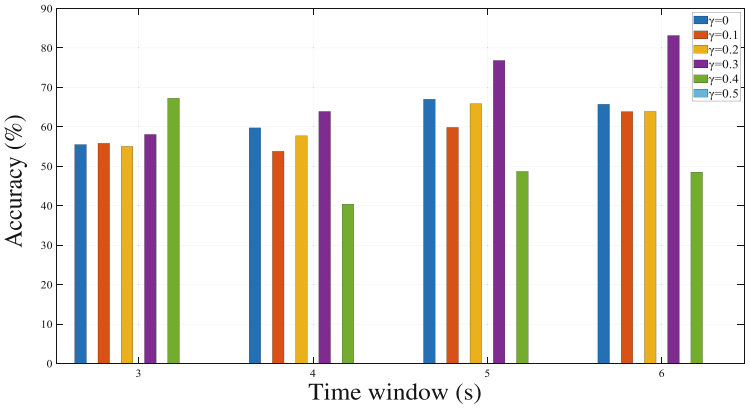


**Fig. 9.** Average signal classification accuracy of all subjects under different time windows and different threshold value $\gamma$.

From the experimental results, it can be seen that in the outdoor environment where the light is complex, three subjects can control the aircraft with a high accuracy (more than 90%) by using the proposed scheme, and the average accuracy of all subjects reaches 83.3%. These conclusions show that the proposed wearable scheme is feasible in complex scenarios.

With the further development of human-machine interface technology and the further improvement of biological signals processing ability, BCIs are gradually coming into the public vision. Its application in the field of human-machine interface and smart healthcare is the inevitable trend of the development of the biological signal processing technology. The improvement of portability and wearbility of BCI equipments can greatly increase the competitiveness of BCI product. Meanwhile, improving the portability and wearability is one of the key technologies to expand the application scenarios of the SSVEP-BCIs. This study combines the respective advantages of SSVEP-BCI and monocular AR micro-display. Through the use of monocular micro-display, the portability and wearability of SSVEP-BCIs can be effectively improved. Compared with the previous

research schemes of using computer monitors and binocular AR smart glasses, the monocular micro-display proposed in this paper has the best portability and wearability. From the experiment results in Sect. 4, the SSVEP stimuli shown in the micro-display has available signal detection accuracy under the CCA-based method. It can be predicted that more portable solutions and more application scenarios for SSVEP-BCIs based on micro-display will be developed in the future.

**Acknowledgments.** The authors' work was supported in part by the Science and Technology Commission Foundation of Shanghai (No. 21JM0010200).

## References

1. Zhang, L., Liang, Y.C., Niyato, D.: 6G visions: mobile ultra-broadband, super internet-of-things, and artificial intelligence. China Commun. **16**(8), 1–14 (2019). https://doi.org/10.23919/JCC.2019.08.001
2. de Oliveira Júnior, W.G., de Oliveira, J.M., Munoz, R., de Albuquerque, V.H.C.: A proposal for internet of smart home things based on BCI system to aid patients with amyotrophic lateral sclerosis. Neural Comput. Appl. **32**(15), 11007–11017 (2018). https://doi.org/10.1007/s00521-018-3820-7
3. Vidal, J.J.: Toward direct brain-computer communication. Ann. Rev. Biophys. Bioeng. **2**(1), 157–180 (1973). https://doi.org/10.1146/annurev.bb.02.060173.001105
4. Mane, R., Chouhan, T., Guan, C.: BCI for stroke rehabilitation: motor and beyond. J. Neural Eng. **17**(4), 041001 (2020). https://doi.org/10.1088/1741-2552/aba162
5. Yan, N., et al.: Quadcopter control system using a hybrid BCI based on off-line optimization and enhanced human-machine interaction. IEEE Access **8**, 1160–1172 (2020). https://doi.org/10.1109/ACCESS.2019.2961246
6. Hwang, H.J., Lim, J.H., Jung, Y.J., Choi, H., Lee, S.W., Im, C.H.: Development of an SSVEP-based BCI spelling system adopting a qwerty-style led keyboard. J. Neurosci. Methods **208**(1), 59–65 (2012). https://doi.org/10.1016/j.jneumeth.2012.04.011
7. Jin, J., Chen, Z., Xu, R., Miao, Y., Wang, X., Jung, T.P.: Developing a novel tactile p300 brain-computer interface with a cheeks-stim paradigm. IEEE Trans. Biomed. Eng. **67**(9), 2585–2593 (2020). https://doi.org/10.1109/TBME.2020.2965178
8. Tidoni, E., Abu-Alqumsan, M., Leonardis, D., Kapeller, C., Fusco, G., Guger, C., Hintermüller, C., Peer, A., Frisoli, A., Tecchia, F., Bergamasco, M., Aglioti, S.M.: Local and remote cooperation with virtual and robotic agents: a p300 BCI study in healthy and people living with spinal cord injury. IEEE Trans. Neural Syst. Rehab. Eng. **25**(9), 1622–1632 (2017). https://doi.org/10.1109/TNSRE.2016.2626391
9. Sreeja, S., Samanta, D.: Classification of multiclass motor imagery EEG signal using sparsity approach. Neurocomputing **368**, 133–145 (2019). https://doi.org/10.1016/j.neucom.2019.08.037
10. Ang, K.K., Guan, C.: EEG-based strategies to detect motor imagery for control and rehabilitation. IEEE Trans. Neural Syst. Rehab. Eng. **25**(4), 392–401 (2017). https://doi.org/10.1109/TNSRE.2016.2646763
11. Sosnik, R., Zur, O.B.: Reconstruction of hand, elbow and shoulder actual and imagined trajectories in 3D space using EEG slow cortical potentials. J. Neural Eng. **17**(1), 016065 (2020). https://doi.org/10.1088/1741-2552/ab59a7

12. Zhang, M., Wang, Z., Hu, H.: A new SSVEP-based BCI utilizing frequency and space to encode visual targets. Sci. China Inf. Sci. **63**(8), 1–3 (2020). https://doi.org/10.1007/s11432-019-2652-6
13. Nakanishi, M., Wang, Y., Chen, X., Wang, Y.T., Gao, X., Jung, T.P.: Enhancing detection of SSVEPs for a high-speed brain speller using task-related component analysis. IEEE Trans. Biomed. Eng. **65**(1), 104–112 (2018). https://doi.org/10.1109/TBME.2017.2694818
14. Xu, Y., Ding, C., Shu, X., Gui, K., Bezsudnova, Y., Sheng, X., Zhang, D.: Shared control of a robotic arm using non-invasive brain-computer interface and computer vision guidance. Robot. Auton. Syst. **115**, 121–129 (2019). https://doi.org/10.1016/j.robot.2019.02.014
15. David, K., Berndt, H.: 6G vision and requirements: is there any need for beyond 5G? IEEE Veh. Technol. Mag. **13**(3), 72–80 (2018). https://doi.org/10.1109/MVT.2018.2848498
16. Zhao, X., Liu, C., Xu, Z., Zhang, L., Zhang, R.: SSVEP stimulus layout effect on accuracy of brain-computer interfaces in augmented reality glasses. IEEE Access **8**, 5990–5998 (2020). https://doi.org/10.1109/ACCESS.2019.2963442
17. Arpaia, P., Duraccio, L., Moccaldi, N., Rossi, S.: Wearable brain-computer interface instrumentation for robot-based rehabilitation by augmented reality. IEEE Trans. Inst. Measure **69**(9), 6362–6371 (2020). https://doi.org/10.1109/TIM.2020.2970846
18. Angrisani, L., Arpaia, P., Esposito, A., Moccaldi, N.: A wearable brain-computer interface instrument for augmented reality-based inspection in industry 4.0. IEEE Trans. Inst. Meas. **69**(4), 1530–1539 (2020). https://doi.org/10.1109/TIM.2019.2914712
19. Daniela, O.R., Verónica, H.I., John, O.G.: SSVEP study in monocular and binocular vision. In: 2019 XXII Symposium on Image, Signal Processing and Artificial Vision (STSIVA), pp. 1–5 (2019). https://doi.org/10.1109/STSIVA.2019.8730241
20. Lin, Z., Zhang, C., Wu, W., Gao, X.: Frequency recognition based on canonical correlation analysis for SSVEP-based BCIS. IEEE Trans. Biomed. Eng. **54**(6), 1172–1176 (2007). https://doi.org/10.1109/TBME.2006.889197
21. Manyakov, N.V., Chumerin, N., Robben, A., Combaz, A., van Vliet, M., Hulle, M.M.V.: Sampled sinusoidal stimulation profile and multichannel fuzzy logic classification for monitor-based phase-coded SSVEP brain-computer interfacing. J. Neural Eng. **10**(3), 036011 (2013). https://doi.org/10.1088/1741-2560/10/3/036011
22. Brainard, D.H.: The psychophysics toolbox. Spatial Vis. **10**(4), 433–436 (1997). https://doi.org/10.1163/156856897X00357